Communication

Two-Step Intercritical Annealing to Eliminate Lüders Band in a Strong and Ductile Medium Mn Steel

JIAWEI MA, QI LU, LI SUN, and YAO SHEN

Lüders band usually apprears in medium Mn steel, and they are difficult to be eliminated without sacrificing the mechanical properties. In this study, a tailored two-step intercritical annealing approach is proposed to eliminate Lüders band and maintain excellent mechanical behavior. A strong ferritic matrix and austenite with appropriate stability are obtained, achieving excellent mechanical behavior. Lüders band is fully removed by the early stress-induced martensitic transformation.

https://doi.org/10.1007/s11661-018-4791-0

Driven by the increasing demands for fuel efficiency and passenger safety in the automotive industry, numerous studies have focused on developing advanced high-strength steels (AHSSs) with excellent mechanical behaviors. Medium Mn steel, alloyed with 4 to 12 wt pct Mn content, has recently been regarded as a promising candidate for third-generation AHSSs.[1–7] This steel is frequently subjected to intercritical annealing after cold rolling (hereafter named one-step intercritical annealing). It is reported that the intercritical annealing temperature remarkably affects its mechanical behavior, and Lüders band tends to appear.[8–13] A combination of high yield strength (YS) and high ductility without the existence of Lüders band is difficult to achieve by one-step intercritical annealing. With a low or medium intercritical annealing temperature, despite the high YS and large total elongation, an unexpected large Lüders strain exists,[9,12] which may give rise to surface roughness and cause potential performance issues during the forming process. On the other hand, with a high intercritical annealing temperature, the steel usually exhibits low YS and decreased total elongation although no Lüders strain is present.[8,11,13]

For medium Mn steel, Lüders band could be caused by the low mobile dislocation density in the ultrafine-grained (UFG) ferritic matrix after intercritical annealing.[11,14] Hence, introducing extra mobile dislocations into the ferritic matrix may be a feasible methodology for preventing Lüders band. It is well known that these extra mobile dislocations can be introduced into adjacent ferrite grains by martensitic transformation of the austenite grains. The martensitic transformation could initiate from either unstable austenite during cooling after intercritical annealing[10] or less unstable austenite during loading before the plastic deformation in ferrite, called stress-induced martensitic transformation.[11,15]

Therefore, excellent mechanical behavior without the appearance of Lüders band could be achieved in a microstructure consisting of an UFG ferritic matrix and large volume fraction of austenite with appropriate stability. The high YS of UFG ferritic matrix ensures the high YS, and austenite with appropriate stability contributes to the elimination of Lüders band and the large total elongation. However, this microstructure is difficult to obtain by traditional one-step intercritical annealing. With a low or medium intercritical annealing temperature, the microstructure consists of an UFG ferritic matrix and some austenite with high stability.[14] However, with a high intercritical annealing temperature, the microstructure consists of a ferritic matrix with increased grain size and a considerable amount of austenite with stability that is too low.[13,16,17]

In the present study, a novel two-step intercritical annealing approach is proposed to achieve the desired microstructure. The cold-rolled medium Mn steel was first subjected to a lower intercritical temperature to produce an UFG ferrite–austenite duplex microstructure and then followed by a higher intercritical temperature to achieve moderate austenite grain growth but negligible ferrite grain growth. This microstructure is demonstrated to achieve an excellent mechanical behavior, meanwhile eliminating the Lüders band and providing a high strain-hardening capacity, which is beneficial for the forming process.

The studied medium Mn steel has a chemical composition of Fe-0.14C-7.14Mn-0.23Si (wt pct). As illustrated in Figures 1(a) and (b), in one-step intercritical annealing, the steel was hot-rolled to a thickness of 3 mm in a temperature range from 1200 °C to 800 °C and cold-rolled to a thickness of 1.4 mm. Then, we annealed the cold-rolled sheet at a low intercritical temperature of 620 °C for 3 minutes. In our designed two-step intercritical annealing, we further added an optimized annealing process at a higher intercritical temperature of 700 °C for about 2 minutes as the second

JIAWEI MA is with the School of Materials Science and Engineering, Shanghai Jiao Tong University, No. 800, Dongchuan Road, Shanghai, China and also with the General Motors China Science Lab, GM(China) Investment Co., Ltd., No. 56, Jinwan Road, Shanghai, China. QI LU and LI SUN are with the General Motors China Science Lab, GM(China) Investment Co., Ltd., Contact e-mail: qi.lu@gm.com YAO SHEN is with the School of Materials Science and Engineering, Shanghai Jiao Tong University. Contact e-mail: yaoshen@sjtu.edu.cn

Manuscript submitted March 16, 2018.
Article published online July 16, 2018

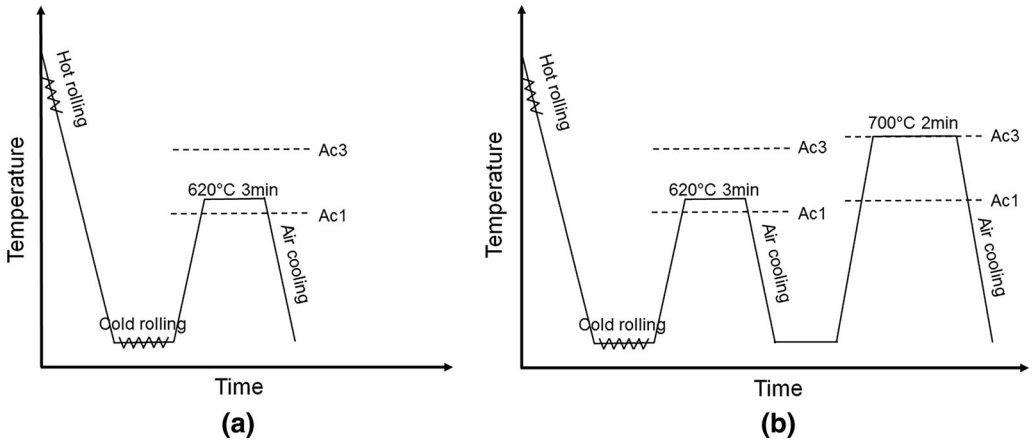

Fig. 1—A schematic illustration of the heat treatment approaches of (*a*) 1S alloy and (*b*) 2S alloy.

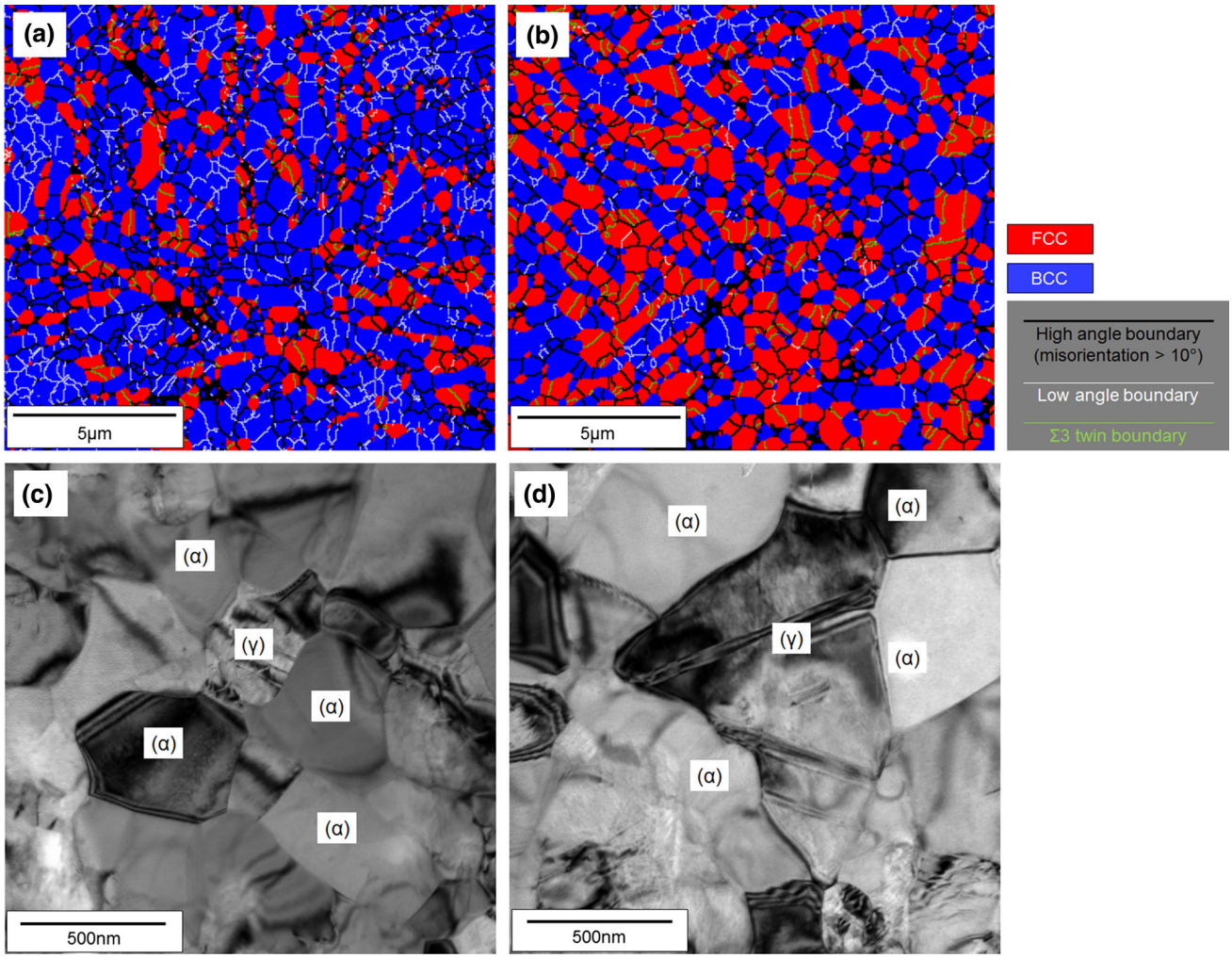

Fig. 2—EBSD phase maps of (*a*) 1S alloy and (*b*) 2S alloy. Ferrite and austenite are represented by blue and red color, respectively. Bright-field TEM images showing the initial microstructure of (*c*) 1S alloy and (*d*) 2S alloy (Color figure online).

step. In the following, they are designated as "1S alloy" and "2S alloy", respectively. Mechanical properties were examined by uniaxial tensile tests at 293 K and 328 K with a nominal strain rate of 1×10^{-3} s^{-1}. Dog-bone-shaped specimens (refer to ASTM E8 standards) were machined with a gauge length of 50 mm along the rolling direction. The strain and strain rate field evolutions during tensile tests were captured by digital image correlation (DIC). The frame rate of the camera was set to be four frames per second. Post-processing was

Table I. Average Grain Size of Ferrite and Austenite Measured by EBSD and Volume Fraction of Austenite Measured by XRD

Materials	Volume Fraction of Austenite (Pct)	Average Austenite Grain Size (μm)	Average Ferrite Grain Size (μm)
1S Alloy	30	0.35	0.58
2S Alloy	45	0.49	0.53

conducted in the Vic-3D software of Correlated Solutions™, Inc. The engineering strains on the tensile curves were all measured by the virtual extensometer in the Vic-3D software. The microstructure was characterized by electron backscatter diffraction (EBSD). EBSD maps were taken by Zeiss Auriga™ 4511-FEG-SEM equipped with an Oxford EBSD detector at an accelerating voltage of 20 kV and a step size of 50 nm. The initial microstructures of 1S alloy and 2S alloy were investigated by transmission electron microscopy (TEM) using a JEOL 2100 F operated at 200 kV. TEM samples were prepared by mechanical polishing and then twin-jet electropolishing at – 20 °C. The volume fraction of austenite was measured by X-ray diffraction (XRD) with Co Kα radiation. Integrated intensities of the $(200)_\alpha$, $(211)_\alpha$, $(200)_\gamma$, $(220)_\gamma$ and $(311)_\gamma$ diffraction peaks were utilized for calculation.

The desired microstructure has been achieved by our designed two-step intercritical annealing approach. Figures 2(a) and (b) presents the phase maps of 1S alloy and 2S alloy, respectively. Table I lists the average grain size of ferrite and austenite measured by EBSD and volume fraction of austenite measured by XRD. Compared to 1S alloy, an UFG ferritic matrix exists with a similar grain size (0.53 *vs* 0.58 μm), larger volume fraction (45 *vs* 30 pct) and larger grain size (0.49 *vs* 0.35 μm) of austenite in 2S alloy. The average ferrite grain size in 2S alloy became slightly smaller because austenite grew into ferrite. Moreover, the content of Mn and C in austenite of 2S alloy should be less than that in austenite of 1S alloy, considering the dilution of the chemical composition caused by the larger volume fraction of austenite. It is well known that austenite's stability is strongly affected by its grain size and chemical composition.[18,19] Therefore, austenite of 2S alloy has a lower stability than that of 1S alloy. However, it should be pointed out that the stability is not as low as that of steels annealed by one-step high intercritical annealing temperature,[13] since the average austenite grain size of 2S alloy is still ultrafine. Figures 2(c) and (d) are the bright-field TEM images showing the initial microstructure of 1S alloy and 1S alloy. It is obvious that both materials have a low dislocation density.

The desired mechanical properties of medium Mn steel are also achieved in 2S alloy. Figure 3 shows the engineering stress–strain curves of 1S alloy and 2S alloy tested at 293 K, respectively, as well as 2S alloy tested at 328 K. The corresponding DIC-computed strain rate evolution maps are illustrated in Figure 4. First, 2S alloy exhibits an excellent tensile behavior, with a YS of 790 MPa and an ultimate tensile strength up to 1334 MPa, showing obvious strain-hardening behavior during plastic deformation. Here, the YS of the sample with Lüders band (1S alloy) is taken as the lower yield

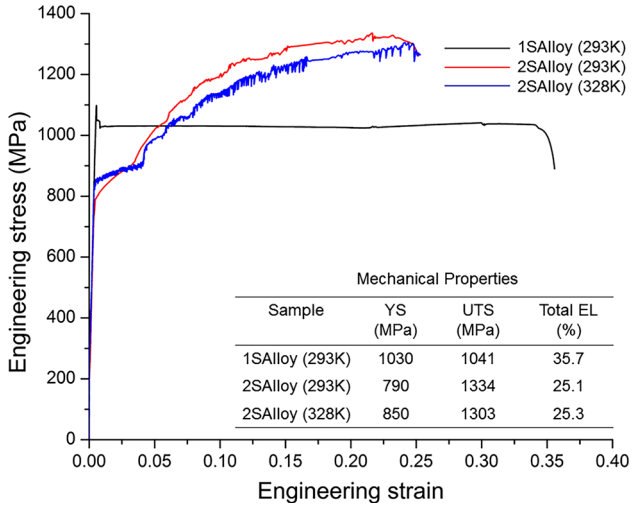

Fig. 3—The engineering stress–strain curves of 1S alloy and 2S alloy with an applied strain rate of 1×10^{-3} s^{-1}.

point, while that of the sample without Lüders band (2S alloy) is taken as the 0.2 pct offset stress. Furthermore, the total elongation has reached 25.1 pct, which is enough for the forming process in the automotive industry. Second, the Lüders band has been eliminated as expected. As shown in Figure 4, the first propagative band of 1S alloy is a Lüders band, while the propagative bands of 2S alloy at 293 K and 328 K are all PLC bands. This could be seen from the characteristics of Lüders band and PLC band. Lüders band corresponds to a stress plateau on the engineering stress–strain curve, which follows the sharp yield point drop and exhibits no strain hardening. In comparison, an obvious strain-hardening behavior is still exhibited on the engineering stress–strain curve when a PLC band exists.[20] Although the PLC band is also a kind of plastic instability phenomenon, the disadvantages it carries are not as severe as those with the Lüders band, for at least two reasons: (1) the degree of strain localization is much lower in 2S alloy than in 1S alloy. The localized plastic strain in the PLC bands of 2S alloy is no more than 5 pct, while that in the Lüders band of 1S alloy is about 22 pct (analyzed based on the DIC-computed strain evolution maps, not shown here), (2) 2S alloy exhibits obvious strain-hardening behavior, while there is almost no strain hardening on the engineering stress–strain curve of 1S alloy. The high degree of strain localization combined with no strain-hardening capacity will significantly deteriorate the formability. Additionally, an unusual increase of the elastic limit is seen in 2S alloy when raising the testing temperature from 293 K to 328 K rather than the usual softening with rising temperature. This phenomenon provides support for our viewpoint

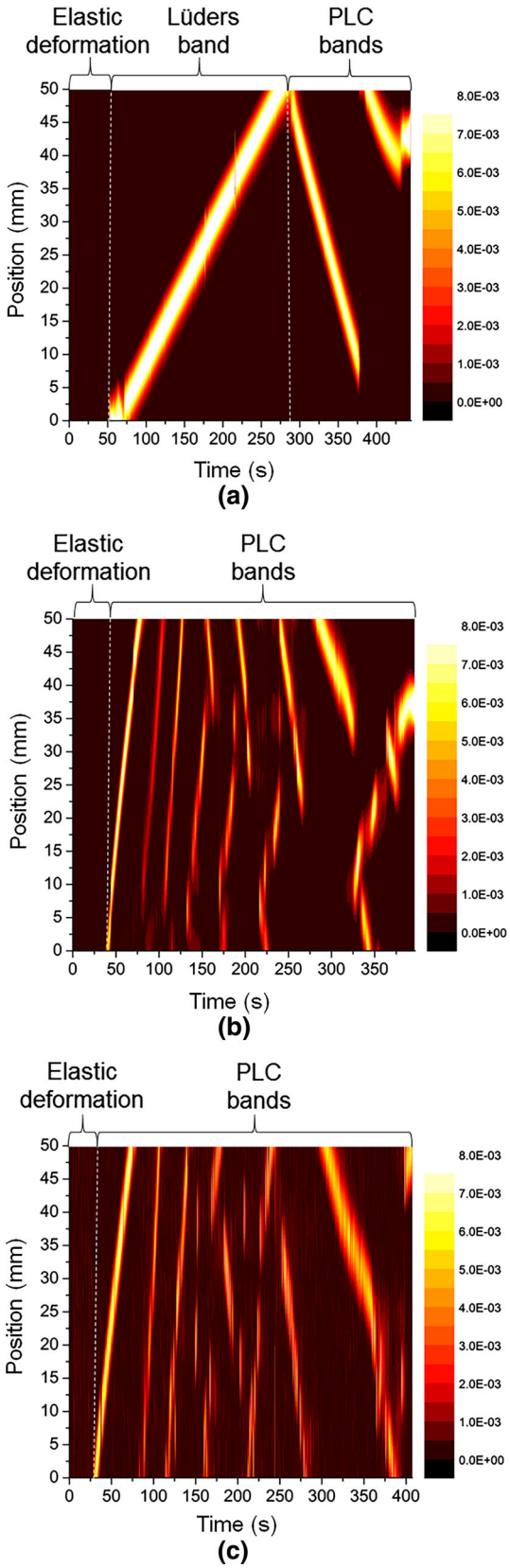

Fig. 4—DIC-computed strain rate evolution maps of (*a*) 1S alloy tested at 293 K, (*b*) 2S alloy tested at 293 K, and (*c*) 2S alloy tested at 328 K. The "position" in the vertical axis is the position in the central line of the parallel section on the tensile specimen.

that stress-induced martensitic transformation occurs before the initiation of plastic deformation in ferrite, which will be described later.

The ideal microstructure of UFG ferrite and medium-grain-sized austenite with appropriate stability is easily achieved by the added second higher temperature intercritical annealing for two reasons. First, in our second higher temperature intercritical annealing, the growth rates of both ferrite and austenite are substantially reduced compared with that in the one-step high-temperature annealing. This is because in the former case the growth of ferrite is solely driven by grain boundary energy reduction, while in the latter case ferrite grows by ferrite/martensite interface migration governed by bulk strain and chemical energy reduction besides the grain boundary movement. The high-temperature austenite grows more slowly in the two-step approach than in the one-step high-temperature annealing because of the big difference in the contributions to and driving force for the growth or transformation. In the one-step high-temperature annealing, the contributions to the increase in the grain size of austenite include the transformation from martensite directly to austenite, and from ferrite to austenite, and the pure grain boundary movement, while the contribution in the high-temperature annealing of the two-step approach solely includes the transformation from ferrite, since martensite is exhausted and austenite is mainly in isolated state after the low-temperature annealing in the two-step approach. Moreover, the driving force for phase transformation from annealed ferrite to austenite is obviously lower than that from cold-rolled martensite to austenite. Second, in our second higher temperature annealing, the growth rate of austenite is faster than that of ferrite, leading to the fast interface migration into adjacent ferrite grains and then obstructing the grain growth of ferrite. This is because at this high temperature, the austenite reversion process is controlled by the easy diffusion of interstitial element C rather than that of the substitutional element Mn.[21]

The achievement of an excellent combination of high strength and large elongation in addition to getting rid of the Lüders band could be attributed to the large amount of austenite with appropriate stability and the UFG ferritic matrix in 2S alloy. First, some austenite with lower stability in 2S alloy can eliminate the Lüders band by introducing mobile dislocations into adjacent ferrite grains *via* stress-induced martensitic transformation early before the initiation of plastic deformation in ferrite. This mechanism for elimination of the Lüders band had been speculated before in some medium Mn steels[11,22]; the current research provides further indirect support. As shown in Figure 3, an unusual increase of the elastic limit exists when raising the testing temperature, contrary to the usual softening upon temperature increasing. Since there is almost no dislocation plasticity behavior at the elastic limit, this unusual phenomenon could not be related to dynamic strain aging. It is known that austenite has a higher stability at 328 K than at 293 K, thus requiring higher stress to initiate the transformation. These facts indicate that the

martensitic transformation is the dominating factor influencing the elastic limit and that it occurs before the dislocation plasticity. In addition, as shown in Figure 2(d), the low dislocation density in the initial microstructure of 2S alloy also helps to support our opinion that Lüders band is eliminated by the early stress-induced martensitic transformation, not by the high mobile dislocation density in ferrite. However, Lüders band tends to be induced in 1S alloy by the low mobile dislocation density in ferrite after intercritical annealing since the austenite in it is too stable and ferrite yields first. Second, the cooperation between the appropriate austenite stability and UFG ferritic matrix results in the high YS of 2S alloy. Appropriate austenite stability ensures that they will not transform into martensite if the stress is too low. UFG ferritic matrix with a high YS allows stress-induced martensitic transformation to occur at a higher stress before the initiation of plastic deformation in ferrite. For the above two reasons, 2S alloy has a high YS of 790 MPa. In comparison, the stability of the austenite produced by one-step intercritical annealing with a high temperature is too low. Though austenite's stability will increase if annealed at a medium intercritical annealing temperature, the coarsening of ferrite will make it yield before the stress-induced martensitic transformation so that the Lüders band reappears.[8,13] Third, the large amount of martensitic transformation provides sufficient strain hardening, which contributes to the large elongation by suppressing the local softening induced by PLC bands.

In summary, a two-step intercritical annealing approach has been proposed, which can eliminate the Lüders band, maintain an excellent tensile behavior and provide enough strain-hardening capability, which is critical for the forming process in the automotive industry. The elimination of Lüders band could be realized by stress-induced martensitic transformation early before the initiation of plastic deformation in ferrite. The excellent mechanical behavior originates from the combination of an UFG ferritic matrix and large volume fraction of austenite with appropriate stability. Finally, this annealing process is possible to incorporate into the real steel production line.

YS acknowledges the support from the National Natural Science Foundation of China (Project Nos. 51471107 and 51671132). JM acknowledges Haiting Liu, Ao Tang from Shanghai Jiao Tong University and Jiachen Pang from General Motors China Science Lab for help with experiments.

REFERENCES

1. D.-W. Suh and S.-J. Kim: *Scripta Mater.*, 2017, vol. 126, pp. 63–67.
2. Y.K. Lee and J. Han: *Mater. Sci. Technol.*, 2014, vol. 31, pp. 843–56.
3. H. Luo, J. Shi, C. Wang, W. Cao, X. Sun, and H. Dong: *Acta Mater.*, 2011, vol. 59, pp. 4002–14.
4. E.J. Seo, L. Cho, and B.C. De Cooman: *Acta Mater.*, 2016, vol. 107, pp. 354–65.
5. Z.H. Cai, H. Ding, R.D.K. Misra, and Z.Y. Ying: *Acta Mater.*, 2015, vol. 84, pp. 229–36.
6. X.G. Wang, L. Wang, and M.X. Huang: *Acta Mater.*, 2017, vol. 124, pp. 17–29.
7. B. Sun, N. Vanderesse, F. Fazeli, C. Scott, J. Chen, P. Bocher, M. Jahazi, and S. Yue: *Scripta Mater.*, 2017, vol. 133, pp. 9–13.
8. P.J. Gibbs, E. De Moor, M.J. Merwin, B. Clausen, J.G. Speer, and D.K. Matlock: *Metall. Mater. Trans. A*, 2011, vol. 42A, pp. 3691–3702.
9. S. Lee, S.-J. Lee, S. Santhosh Kumar, K. Lee, and B.C.D. Cooman: *Metall. Mater. Trans. A*, 2011, vol. 42A, pp. 3638–51.
10. S. Lee and B.C. De Cooman: *Metall. Mater. Trans. A*, 2013, vol. 44A, pp. 5018–24.
11. B.C. De Cooman, P. Gibbs, S. Lee, and D.K. Matlock: *Metall. Mater. Trans. A*, 2013, vol. 44A, pp. 2563–72.
12. D.W. Suh, J.H. Ryu, M.S. Joo, H.S. Yang, K. Lee, and H.K.D.H. Bhadeshia: *Metall. Mater. Trans. A*, 2013, vol. 44A, pp. 286–93.
13. K. Steineder, D. Krizan, R. Schneider, C. Béal, and C. Sommitsch: *Acta Mater.*, 2017, vol. 139, pp. 39–50.
14. J. Han, S.-J. Lee, J.-G. Jung, and Y.-K. Lee: *Acta Mater.*, 2014, vol. 78, pp. 369–77.
15. P.J. Gibbs, B.C. De Cooman, D.W. Brown, B. Clausen, J.G. Schroth, M.J. Merwin, and D.K. Matlock: *Mater. Sci. Eng. A*, 2014, vol. 609, pp. 323–33.
16. S. Lee and B.C. De Cooman: *Metall. Mater. Trans. A*, 2014, vol. 45A, pp. 5009–16.
17. J.M. Jang, S.J. Kim, N.H. Kang, K.M. Cho, and D.W. Suh: *Met. Mater. Int.*, 2009, vol. 15, pp. 909–16.
18. S. Lee, S.-J. Lee, and B.C. De Cooman: *Scripta Mater.*, 2011, vol. 65, pp. 225–28.
19. E. Jimenez-Melero, N.H. van Dijk, L. Zhao, J. Sietsma, S.E. Offerman, J.P. Wright, and S. van der Zwaag: *Scripta Mater.*, 2007, vol. 56, pp. 421–24.
20. E. Rizzi: *Int. J. Plast.*, 2004, vol. 20, pp. 121–65.
21. M. Calcagnotto, D. Ponge, and D. Raabe: *ISIJ Int.*, 2008, vol. 48, pp. 1096–1101.
22. J.H. Ryu, J.I. Kim, H.S. Kim, C.-S. Oh, H.K.D.H. Bhadeshia, and D.-W. Suh: *Scripta Mater.*, 2013, vol. 68, pp. 933–36.